Available online at www.sciencedirect.com
ScienceDirect
Journal of Catalysis 251 (2007) 497–506
JOURNAL OF CATALYSIS
www.elsevier.com/locate/jcat

Hydrogenation of tetralin on silica–alumina-supported Pt catalysts II. Influence of the support on catalytic activity

M.F. Williams [a], B. Fonfé [a], C. Woltz [a], A. Jentys [a], J.A.R. van Veen [b], J.A. Lercher [a,*]

[a] *TUM, Institute for Chemical Technology 2, Lichtenbergstraße 4, D-85747 Garching, Germany*
[b] *Shell International Chemicals B.V, Badhuisweg 3, 1031 CM Amsterdam, The Netherlands*

Received 5 March 2007; revised 2 June 2007; accepted 8 June 2007

Available online 10 August 2007

Abstract

The interactions between an oxidic support and Pt particles were explored in a series of platinum catalysts supported on amorphous silica–alumina used for the hydrogenation of tetralin and the hydrogenolysis of neopentane. The activity of the nanosized Pt particles increased with increasing intermediate electronegativity of the support for all supports with accessible Lewis acid sites. A compensation effect between the preexponential factor and the apparent energy of activation was observed for both reactions, attributed to the stronger adsorption of the reactants and intermediates on Pt induced by the increasingly electronegative supports. The product distribution in tetralin hydrogenation also points to stronger adsorption on Pt with increasing intermediate electronegativity of the support. X-ray absorption near-edge structure (XANES) findings indicate that the stronger interaction of the reactants is related to a reduced electron density on the platinum particles.

Keywords: Platinum; Catalysts; Nanoparticles; Amorphous silica–alumina; Hydrogenation of tetralin; Hydrogenolysis of neopentane; Metal–support interaction; XANES

1. Introduction

The formation of diesel particulates in automobile exhaust gases depends on the content of aromatic hydrocarbons in the fuel. The maximum level of these particulates will be strictly limited in projected environmental regulations [1]. Currently, hydrogenation is one of the most important routes for reducing the concentration of aromatics, leading to fuel components with high cetane numbers. Conventional diesel hydrotreating based on sulfided NiMo, CoMo, and NiW/Al_2O_3 catalysts is effective in decreasing the concentration of S- and N-compounds; however, insufficient reduction levels of aromatics in the diesel fraction are obtained unless severe operating conditions are applied (i.e., high temperature and hydrogen partial pressure, low space velocity) [2–4].

A more economic hydrotreating process is achieved by a follow-up deep catalytic hydrotreating (DHT) based on noble metal catalysts [5–7]. Unfortunately, however, although the catalysts are very active in the hydrogenation of aromatics, noble metals also are very sensitive to residual amounts of sulfur and nitrogen compounds present in the feedstock. It has been shown that using acidic supports increases the catalyst resistance toward sulfur poisoning [8–10]. However, the functions of different kinds of acid sites (Brønsted vs Lewis acidity), and their optimal concentrations and strengths, remain unclear. An unambiguous model for the action of these catalysts requires a detailed description of the structural relationship between the support and noble metal particles.

For the hydrogenation of aromatic molecules in the absence of poisons, the acidity of the support has been shown to have a significant influence on the activity of supported metal catalysts. The rate of benzene hydrogenation has been reported to increase with increasing acid site concentration, which was generally explained by an increase in metal electron deficiency [11]. However, Vannice and co-workers [12,13] attributed the increase in aromatic hydrogenation activity of Pt and Pd supported on acidic supports compared with catalysts on inert supports to the presence of additional hydrogenation sites in the

* Corresponding author. Fax: +49 89 28913544.
E-mail address: johannes.lercher@ch.tum.de (J.A. Lercher).

0021-9517/$ – see front matter
doi:10.1016/j.jcat.2007.06.010

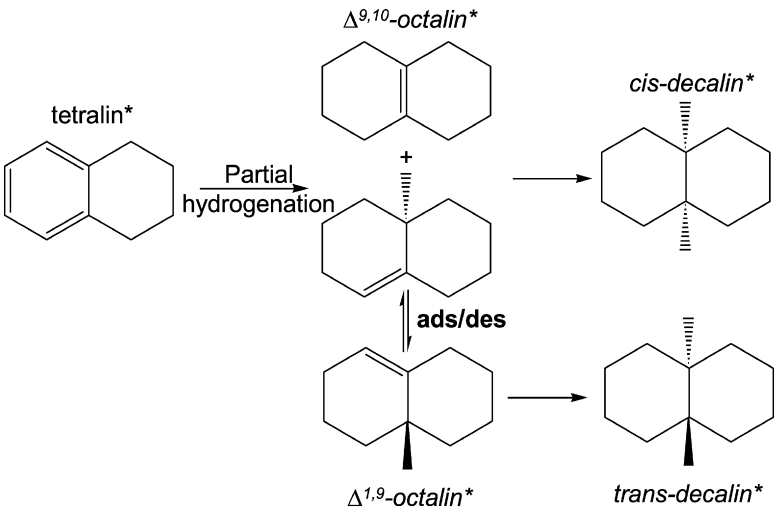

Fig. 1. Stepwise hydrogenation of an adsorbed tetralin molecule to *cis*- and *trans*-decalin.

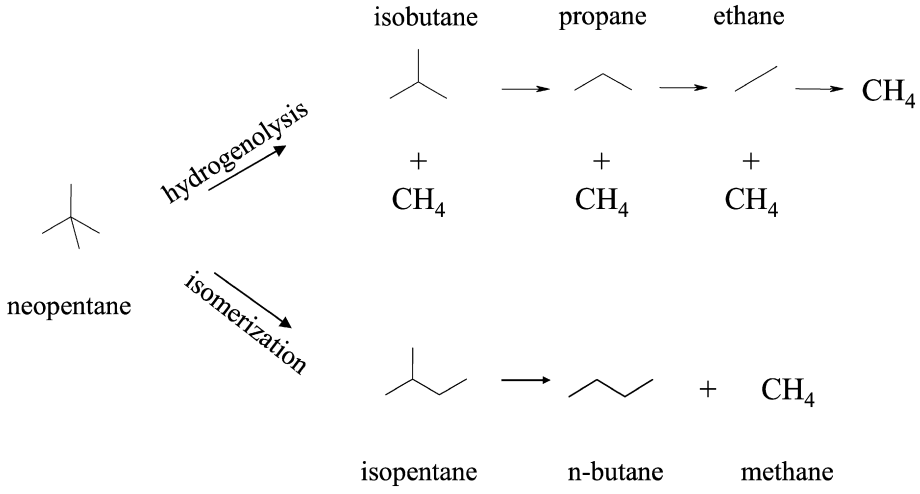

Fig. 2. The reaction network of the neopentane hydrogenolysis (consecutive reactions take place only on the metal sites).

metal–acid interfacial region, contributing to the overall rate of aromatic hydrogenation.

In the present study, we explored the different explanations accounting for the increase in activity by studying a series of platinum nanoparticles supported on amorphous silica–alumina (ASA) with varying amounts of alumina (100, 55, 20, 5, and 0 wt%), in relation to the acidity and electronegativity of the support with no poison in the feed. The hydrogenation of tetralin and hydrogenolysis of neopentane were carried out as probe reactions. Tetralin is a typical molecule targeted in hydrodearomatization (HDA) [14–16]. Under the reaction conditions of the study ($p_{H_2} = 50$ bar, $T < 473$ K), formation of the hydrogenated products (i.e., *cis*- and *trans*-decalin) is thermodynamically strongly favored [17]. Hydrogenation of C=C double bonds on metals should be intrinsically *cis* in character [18]; however, the formation of *trans*-decalin is always observable [19]. According to Weitkamp [20], this depends on the consecutive desorption and readsorption of the partially hydrogenated intermediate, $\Delta^{1,9}$-octalin, as shown in Fig. 1.

Any factors that reduce the strength of interaction of the olefinic intermediate with the surface also will favor the selectivity to the *trans*-isomer. Therefore, the *cis*- to *trans*-selectivity can be considered an indication of the electronic state of the Pt particles [21,22].

To be even more specific, the activity of platinum nanoclusters can be examined by the hydrogenolysis of neopentane, a reaction that depends exclusively on the catalytic activity of platinum [23,24]. This path is intrinsically monofunctional, because neopentane cannot form an alkene intermediate and protolytic cracking of neopentane is not observed below 573 K [25]. Fig. 2 depicts the possible reaction products associated with either hydrogenolysis (i.e., methane and isobutane) or isomerization (i.e., isopentane).

The electronic properties of platinum particles on the different ASA carriers were determined by X-ray absorption spectroscopy. The intensity of the peak above the absorption edge is affected by the type of metal and its chemical state of the atoms, the measuring temperature, the presence of an adsorbate on the surface of the metal particles, the size of the metal clusters, and the support [26–29]. The purpose of the present study is to gain

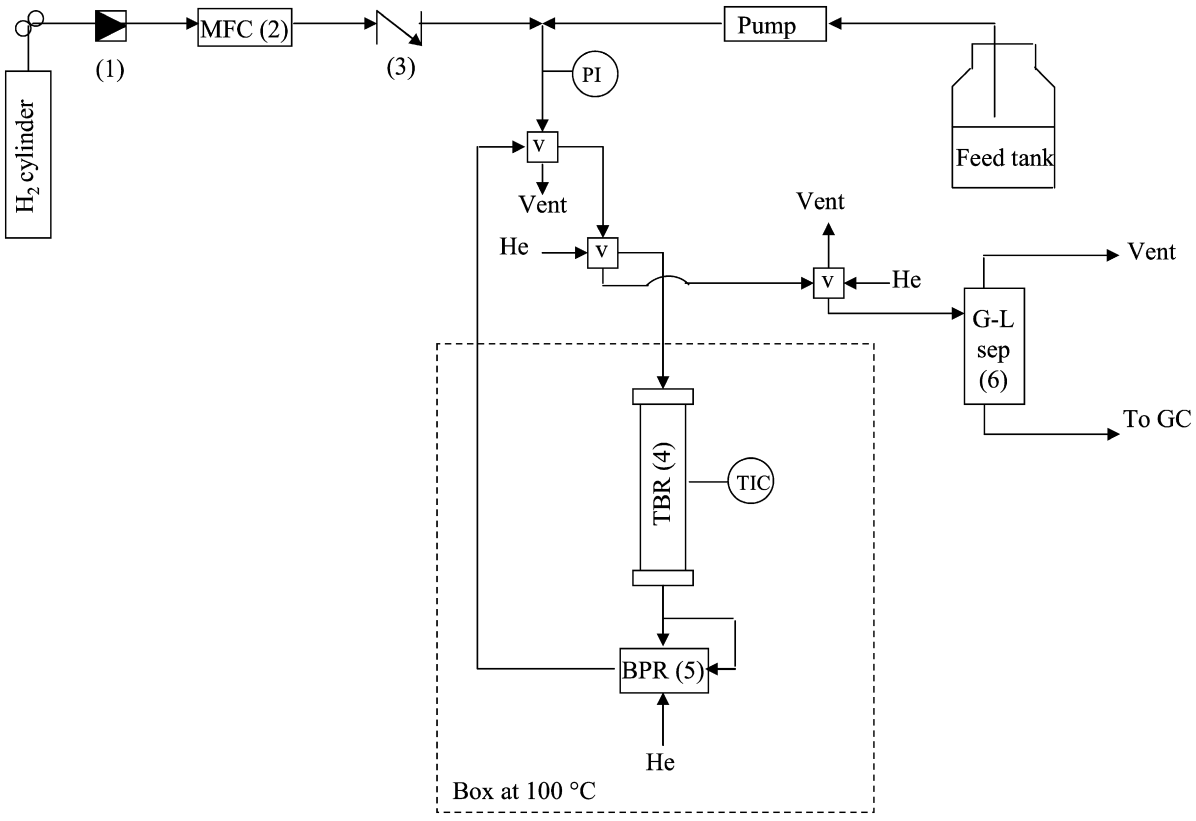

Fig. 3. Simplified flow diagram of the continuous hydrogenation testing unit: (1) pressure reducer, (2) mass flow controller, (3) check valve, (4) trickle bed reactor, (5) back pressure regulator, (6) gas–liquid separator.

insight into the effect of the support on the electronic properties of the Pt nanoclusters investigated by various probe reactions and X-ray absorption spectroscopy.

2. Experimental

2.1. Catalytic testing

All chemicals were obtained from commercial suppliers and used as provided: tetralin (Aldrich, 99% GC assay), hexadecane (Merck, >99% GC assay), *n*-tetradecane (Aldrich, >99% GC assay), *cis*- and *trans*-decalin (Aldrich, 99% GC assay), hydrogen (Air Liquide, >99.999%), and neopentane (Messer Griesheim GmbH, 5 vol% in hydrogen). The hydrogenation of tetralin (20 wt% in a mixture with hexadecane and *n*-tetradecane, reflecting typical concentrations in diesel fractions) was carried out in a trickle-bed reactor operated in continuous down-flow mode, as depicted in Fig. 3.

The reactor was filled with catalyst ($d = 300$–600 μm) diluted with SiC (ratio = 0.01–0.03 g_{cat}/g_{SiC}) to ensure a homogeneous thermal distribution. To avoid entrance effects, two inert layers (i.e., SiC and glass wool) were placed on the top and the bottom of the catalyst bed. The liquid feed and hydrogen were dosed by an HPLC pump (Gilson model 5cc) and a Bronkhorst EL-FLOW mass flow controller, respectively. Both reactants were mixed before they entered the reactor. Varying the amount of catalyst and the total flow rate while keeping the space velocity constant and with catalysts of different particle diameters led to unmodified conversion values, confirming the absence of external transport limitations and intraparticle concentration gradients. The performance of the reactor and the accuracy of the analytical method were studied by feeding the organic solution to the reactor filled with SiC, operating at 463 K and 50 bar hydrogen pressure. Formation of unexpected products was not detected, with a recovery percentage of 99% tetralin. The chosen solvents hexadecane and *n*-tetradecane did not react under the applied reaction conditions.

During the experiment, a number of samples were collected for off-line gas chromatography. The analysis was carried out with a HP 6890 gas chromatograph equipped with an Agilent DB-1701 column. *n*-Tetradecane (11.5 wt% in the feed) was used as the internal standard. Before the activity testing, the catalysts were reduced in hydrogen ($p = 1$ bar, flow rate 30 $cm^3\,min^{-1}$, 2 h at 588 K). To preserve the high metal dispersion, a very slow heating rate of 0.41 $K\,min^{-1}$ was applied to reach the final temperature for reduction. If not noted otherwise, the catalytic reactions were carried out at 453 K and 50 bar hydrogen pressure with a weight hourly space velocity (WHSV) range of 90–250 h^{-1}. The variation in space velocity was achieved by changing the amount of catalyst and/or the flow rate while maintaining a constant molar ratio of H_2 to the feed of 20.5. To determine the apparent energy of activation ($E_{a(exp)}$), hydrogenation was carried out at 433, 443, 453, and 463 K at a WHSV of 125 h^{-1} and a hydrogen pressure of 50 bar.

The neopentane hydrogenolysis was studied in a set of 20 parallel reactors controlled by individual digital mass flow meters and pressure regulators [30]. The catalyst samples, di-

Table 1
Characterization of the supported Pt catalysts: Chemical composition, textural properties and intermediate electronegativity of the support according to Sanderson (S_{int})

Catalyst	Composition (wt%)			Acidity (mmol g^{-1})		EXAFS particle model Pt size (nm)	S_{int}
	Pt	SiO_2	Al_2O_3	BAS	LAS		
Pt/Al_2O_3	0.78	0.0	99.2	0.000	0.14	0.6	2.70
Pt/ASA (55/45)	0.82	46.2	53.0	0.02	0.13	0.8	2.86
Pt/ASA (20/80)	0.81	78.8	20.4	0.04	0.09	0.7	2.98
Pt/ASA (5/95)	0.78	94.9	4.3	0.03	0.07	0.8	3.04
Pt/SiO_2	1.03	99.0	0.0	0.00	0.000	1.4	3.05

luted with SiC, were prereduced according to the procedure described above, and a neopentane/hydrogen blend with a $mol_{neopentane}/mol_{H_2}$ ratio of 5/95 was fed into the system. The temperature was varied between 563 and 588 K and the total gas flow was varied between 5 and 25 $cm^3\ min^{-1}$, whereas the total pressure was set to 1 bar. An Agilent GC M200 micro-gas chromatograph was used to analyze the products of hydrogenolysis.

2.2. Extended X-ray absorption fine structure

X-ray absorption spectra were collected at beamline X1 at HASYLAB, DESY, Hamburg, Germany. The storage ring was operated at 4.5 GeV and an average current of 100 mA. The Si (311) double-crystal monochromator was detuned to 60% of the maximum intensity to minimize the contributions of higher harmonics in the X-ray beam. The fresh catalysts were prepared as self-supporting wafers and reduced in situ before the measurements (H_2, $T = 588$ K for 2 h). The X-ray absorption spectra were collected at the Pt L_{III} edge (11,564 eV) at 323 K. For XANES analysis, the scattering background was subtracted using a second-order polynomial function, and all spectra were normalized to unity. The edge position was calibrated using the spectra of a Pt foil measured simultaneously. The intensities of the peak above the absorption edge were obtained from numeric integration of the peak areas. The Viper software was used to analyze the data sets [31].

3. Results and discussion

3.1. Characterization of the supported Pt catalysts

The details of the nature, concentration, strength, and origin of different types of acid sites present in the catalysts have been reported elsewhere [32]. The bulk and surface characterization of the supported platinum catalysts, along with the particle sizes of the Pt clusters, are summarized in Table 1.

All supports had mesoporous structure; thus, intraporous diffusion limitations of the bulky aromatic molecules were not expected. It should be noted that with increasing SiO_2/Al_2O_3 ratio in the catalysts, a maximum concentration of Brønsted acid sites (Pt/ASA 20/80) and decreased concentration of Lewis acid sites was observed. The silica-supported Pt catalyst was used as a neutral reference material.

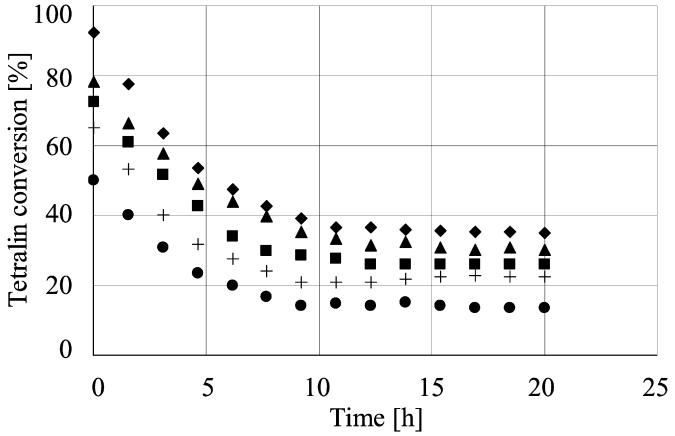

Fig. 4. Hydrogenation of tetralin over Pt/ASA (20/80) at 453 K. WHSV = 90 h^{-1} (◆), 115.4 h^{-1} (▲), 123.8 h^{-1} (■), 141.7 h^{-1} (+) and 249.9 h^{-1} (●).

As shown in previous studies, the average metal cluster sizes determined by XAFS were small and similar for all of the different catalysts except Pt/SiO_2 (see Table 1) [32]. Moreover, the particle size distribution was narrow as confirmed by TEM. This leads to the conclusion that the localized effect of the acid sites on the catalytic properties of the Pt nanoclusters could be investigated without taking into account varying metal particle sizes. Furthermore, the intermediate electronegativity of the support (i.e., the Sanderson electronegativity [33]) increases with increasing concentration of silica in the mixed oxides, and thus the value can be used to compare properties of the catalysts studied.

3.2. Hydrogenation of tetralin

Tetralin hydrogenation was the predominant reaction (see the reaction scheme in Fig. 1) for all catalysts. Secondary reactions on the acid sites (e.g., isomerization, hydrocracking) were hardly observed. Apparently, up to 463 K, the acid sites of the support did not catalyze byproduct formation. It was further observed that the carbon mass balance in the liquid phase was close to 100%; thus no reaction products were present in the gas phase. Typical conversion profiles in dependence of time on stream (TOS) for various residence times are shown in Fig. 4.

At all residence times investigated, the initial conversion of tetralin decreased within the first 15 h and reached a constant level at ca. 20 h. For further kinetic analysis, the activity at a residence time of 250 h^{-1} at 20 h time on stream was used. The rate of hydrogenation of tetralin increased with increasing Sanderson electronegativity for all alumina-containing catalysts (Fig. 8). Notably, the activity on Pt/SiO_2 was the lowest of all of the materials studied.

A first-order dependence of the activity on the hydrocarbon concentration was used to describe the kinetics of the hydrogenation of tetralin at steady-state reaction conditions,

$$-\ln(1 - X_{tet}) = \frac{k}{WHSV}, \quad (1)$$

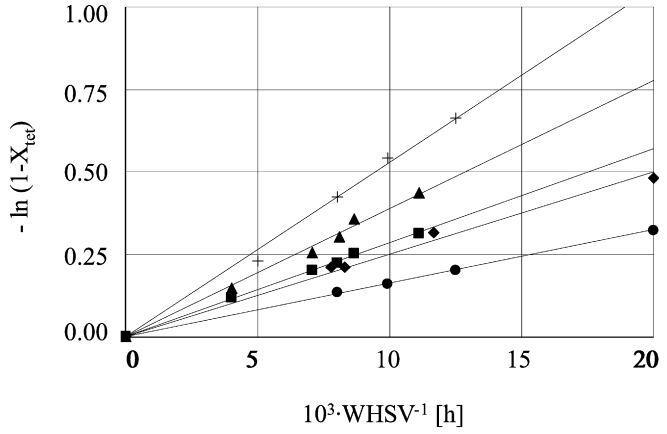

Fig. 5. Pseudo-first-order kinetic fitting of the hydrogenation of tetralin over Pt/Al_2O_3 (◆), Pt/ASA (55/45) (■), Pt/ASA (20/80) (▲), Pt/ASA (5/95) (+), and Pt/SiO_2 (●) at 453 K.

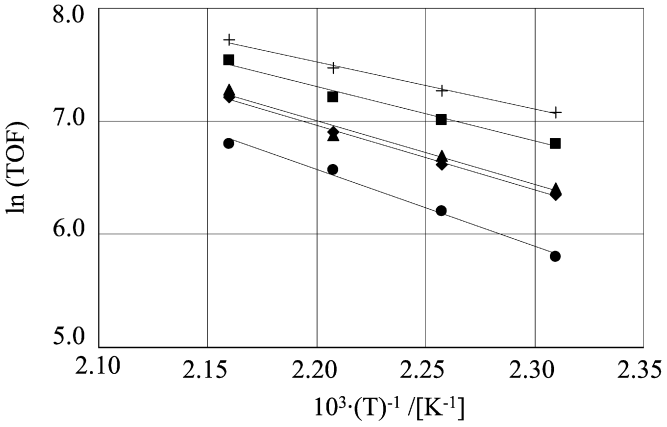

Fig. 6. Arrhenius plots over Pt/Al_2O_3 (◆), Pt/ASA (55/45) (■), Pt/ASA (20/80) (▲), Pt/ASA (5/95) (+), and Pt/SiO_2 (●) in the temperature range from 433 to 463 K.

where X_{tet} is the conversion of tetralin at steady state and k is the product of the surface reaction rate constant and the reactant adsorption constants) (also see [34–37]). A typical fitting procedure is reported in Fig. 5.

An Arrhenius plot (Fig. 6) was used to determine the apparent energy of activation ($E_{a(exp)}$) in the hydrogenation of tetralin over different ASA-supported Pt catalysts. The $E_{a(exp)}$ of Pt/Al_2O_3, Pt/ASA (55/45), Pt/ASA (20/80), and Pt/ASA (5/95) was 48, 47, 40, and 35 kJ mol^{-1}, respectively, demonstrating that the $E_{a(exp)}$ decreased with increasing concentration of silica in the support. The lower activation energy for the materials containing more silica indicates that the Pt clusters are more active on more electronegative supports. Over the Pt/SiO_2, the highest apparent energy of activation (i.e., 57 kJ mol^{-1}) among the catalysts studied was observed, confirming the need for the presence of Lewis acid sites in the support to exert a marked influence on the Pt properties. Note that SiO_2 was the only support that did not show Lewis acidity during sorption of pyridine.

The further analysis of the Arrhenius relation reveals a linear dependence between $E_{a(exp)}$ and $A_{(exp)}$ for the materials investigated (Fig. 7). Such linear correlation is termed *compensation behavior*.

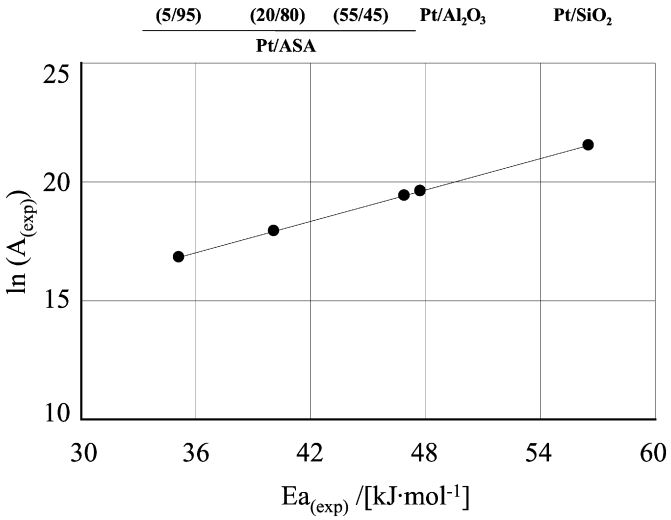

Fig. 7. Constable plot of $\ln(A_{(exp)})$ in dependence on $E_{a(exp)}$ found for the hydrogenation of tetralin over of Pt supported on alumina, ASA and silica carriers.

The observation of a compensation effect suggests that either in an equilibrated reaction step or in the actual rate-determining step, the greater the entropy loss through the equilibrium reaction or in reaching the transition state, the lower the reaction enthalpy or the energetic barrier of the transition state. For a detailed discussion, see the review by Bond et al. [38] on the compensation phenomena in heterogeneous catalysis.

In the present case (i.e., for a first-order reaction), the apparent activation energy is the sum of the true activation energy (E_a) and the enthalpy of adsorption (ΔH_{ads}),

$$E_a = E_{a(exp)} - \sum n_i \Delta H_i . \quad (2)$$

Consequently, the apparent rate constant is actually the product of the true rate constant and the adsorption equilibrium constants of the reactant, that is, tetralin and hydrogen. Thus, the preexponential factor $A_{(exp)}$ contains the entropic part of the adsorption equilibrium constant and the true pre-exponential factor A (containing the transition entropy of the rate-determining step) of the Arrhenius equation of the hydrogenation reaction. Without additional information, the reason for the compensation effect cannot be determined. In turn, it is impossible to accurately determine the entropy, enthalpy, and equilibrium constant of tetralin or decalin adsorption, because the metal fraction on the overall surface is very small (approximately 4 metal particles per 1000 nm^2). Following the rationale in Ref. [38] and in agreement with references [39,40], the changes in $E_{a(exp)}$ are attributed primarily to variations in the adsorption enthalpies of tetralin.

If this holds true, then the decrease in $E_{a(exp)}$ calculated for the more active Pt nanoclusters can be attributed to the increased heat of adsorption of tetralin on the increasingly electron-deficient Pt. Consequently, the increasing strength of adsorption reduces the translation and rotational degrees of freedom, thus leading to a lower entropy of the adsorbed state, which lowers the preexponential factor ($A_{(exp)}$) in the overall

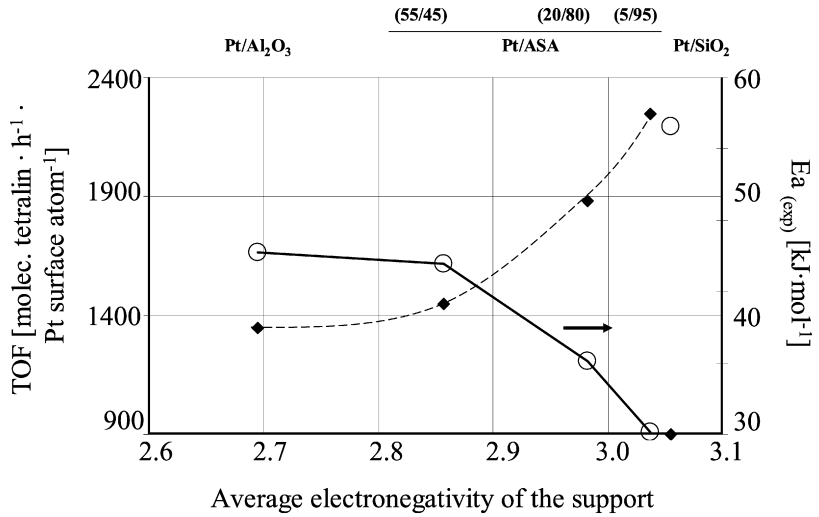

Fig. 8. Changes of the apparent energy of activation and the rate of tetralin hydrogenation (463 K) over Pt catalysts supported on carriers exhibiting different average electronegativities (Sanderson electronegativity).

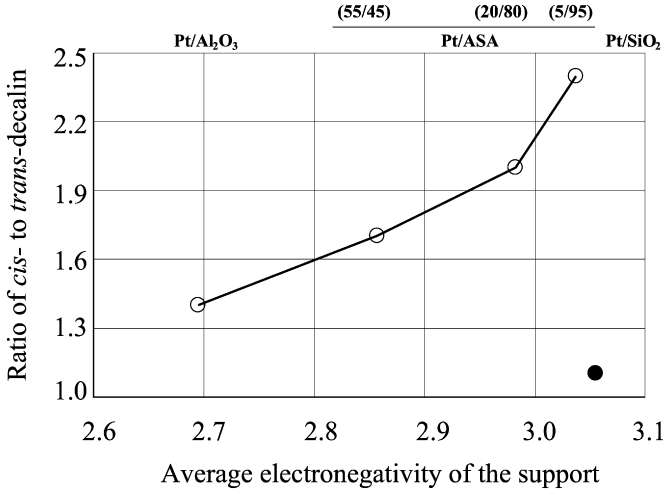

Fig. 9. Dependence of the *cis*- to *trans*-decalin selectivity on the intermediate support electronegativity of the Pt catalysts at approximately 21% conversion level of tetralin ($T = 453$ K, 50 bar).

Arrhenius equation. Fig. 8 shows that the lower the apparent energy of activation of the reaction, the higher the intermediate electronegativity of the support. In line with previous observations, Pt/SiO_2 was again the exception to this correlation.

A further indication toward a stronger bonding of reactants to the increasing electron deficiency of Pt nanoparticles is obtained from the *cis*-/*trans*-selectivity of the final hydrogenation product decalin. The ratio of the *cis*- to the *trans*-decalin increased as the intermediate electronegativity of the support increased with increasing SiO_2 concentrations in the support (Fig. 9).

Analysis of the intermediates and the final selectivities showed that the latter depended critically on the concentration of the isomer in the last hydrogenation step. Two isomers appear to determine the selectivity. If $\Delta^{9,10}$-octalin is more abundant, then *cis*-decalin is formed in larger concentrations, whereas if $\Delta^{1,9}$-octalin is more abundant, then *trans*-decalin is formed preferentially. The $\Delta^{9,10}$-octalin most likely allows for stronger interaction of the central double bond with the metal surface.

To exclude the change of the isomer ratio due to the thermodynamically driven shift of the *cis*- to *trans*-products after secondary readsorption of decalin, a blank experiment was performed. In this experiment, the temperature range, pressure, and WHSV were similar to those used in the tetralin hydrogenation experiments. Instead of 20 wt% tetralin, 20 wt% of either *cis*- or *trans*-decalin was mixed into the feed. Because decalin was not isomerized under the reaction conditions, we can assume that the selectivities observed were controlled by the hydrogenation reaction.

Because the weaker adsorption of tetralin on the metal favors the formation of the *trans* isomer, whereas a stronger adsorption will lead directly to the formation of *cis*-decalin, we conclude that the higher concentration of *cis*-decalin with increasing average electronegativity of the support leads to stronger binding of the reactant and intermediates to the metal surface. Pointing to a more electrophilic- or electron-deficient Pt, this is in line with earlier observations of acidic supports on nanosized platinum particles [41]. Platinum supported on silica, which exhibited the highest average electronegativity among the different supports, did not follow this trend, strongly indicating that Lewis acidity is essential to induce an electronic metal support effect.

3.3. Hydrogenolysis of neopentane

The hydrogenolysis of neopentane, a reaction that is catalyzed only by the metallic function, was used to probe properties of the Pt particles. Under the reaction conditions used, the conversion level decreased initially with time on stream, followed by a period of constant conversion. Thus, all rates were determined after an induction period of 2 h time on stream. The typical product distribution at different conversion levels is shown in Fig. 10.

Almost the same product distribution was observed over all of the catalysts tested, including the formation of methane,

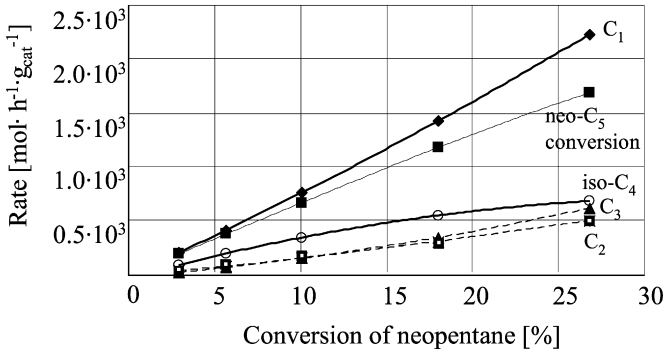

Fig. 10. Product distribution ($T = 588$ K, WHSV = 0.5–2.5 h^{-1}) vs neopentane conversion over Pt/ASA (5/95).

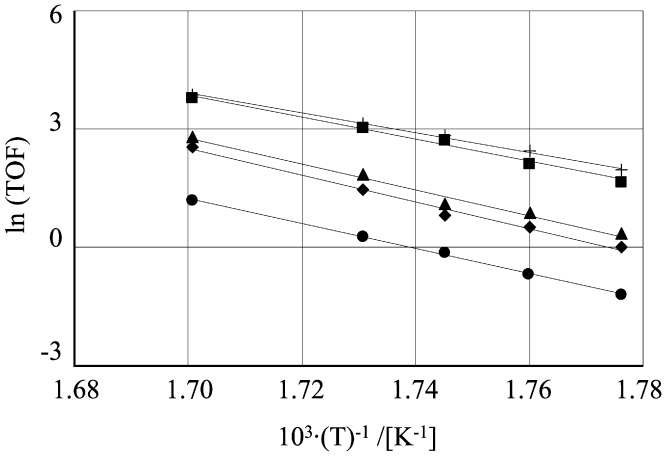

Fig. 11. Arrhenius fitting obtained for the hydrogenolysis of neopentane over Pt/ASA (5/95) (+), Pt/ASA (55/45) (■), Pt/ASA (20/80) (▲), Pt/Al_2O_3 (◆), and Pt/SiO_2 (●) in the temperature range from 563 to 588 K.

ethane, propane, and isobutane as primary reaction products. Thus, only products of hydrogenolysis were present, whereas acid-catalyzed isomerization reactions (i.e., isopentane formation) did not occur. The determination of the apparent activation energy of activation from the Arrhenius equation is shown in Fig. 11. The TOF of the neopentane hydrogenolysis (588 K) and the values of the apparent energy of activation of the different Pt-supported catalysts are compared in Fig. 12. With increasing electronegativity of the support, the rate of neopentane hydrogenolysis increased while $E_{a(exp)}$ decreased, that is, 284, 273, 234, and 209 kJ mol^{-1} for Pt/Al_2O_3, Pt/ASA (55/45), Pt/ASA (20/80), and Pt/ASA (5/95), respectively, in the same order. Again, the Pt/SiO_2 catalyst with $E_{a(exp)} = 265$ kJ mol^{-1} was outside the trend discussed above, similar to that for the hydrogenation of tetralin. It is important to note that a significant reduction in the apparent energy of activation between the alumina-supported and ASA-supported (5/95) platinum (i.e., $\Delta E_{a(exp)} = 75$ kJ mol^{-1}) was observed.

In analogy to the discussion of the tetralin hydrogenation, the increased activity of the Pt catalysts with increasing intermediate electronegativity of the support is attributed to a stronger sorption of neopentane. Note that similar observations in the hydrogenolysis of neopentane have been reported for different metals supported on acidic carriers [42].

It is interesting to note that in this case, a compensation effect also was observed. As for the compensation effect observed for tetralin, we attribute the compensation to the direct relationship between the stronger heat of adsorption of neopentane and the lower entropy in the adsorbed state. Thus, on the more electron-deficient metal particles, the heat of adsorption increases in parallel with the loss of entropy of neopentane. Note that such effects have been observed for hydrogenolysis in several instances [20,27,31,43].

The question now arises as to whether the impact of the support on the Pt particles is similar for a facile reaction, such as the hydrogenation of an aromatic molecule and the structurally more demanding reaction of neopentane hydrogenolysis. The relationship between the catalytic activity for the hydrogenolysis of neopentane and the hydrogenation of tetralin, plotted in Fig. 13, shows a linear positive correlation between the two rates, indicating that the variation in the electronegativity of the support has the same effect on both reactions.

Because the hydrogenolysis of neopentane is known to be a reaction catalyzed solely by the metal, we conclude that both

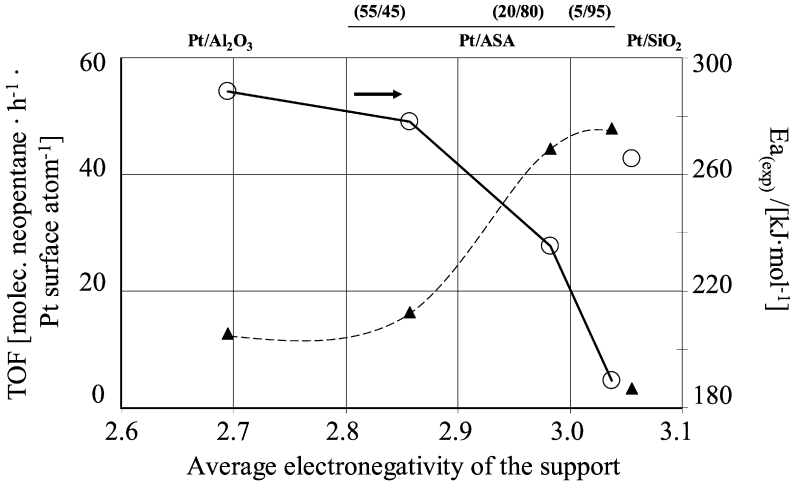

Fig. 12. Changes in the apparent energy of activation and in the TOF of neopentane hydrogenolysis (588 K) over Pt catalysts supported on carriers exhibiting different average electronegativities (Sanderson electronegativity).

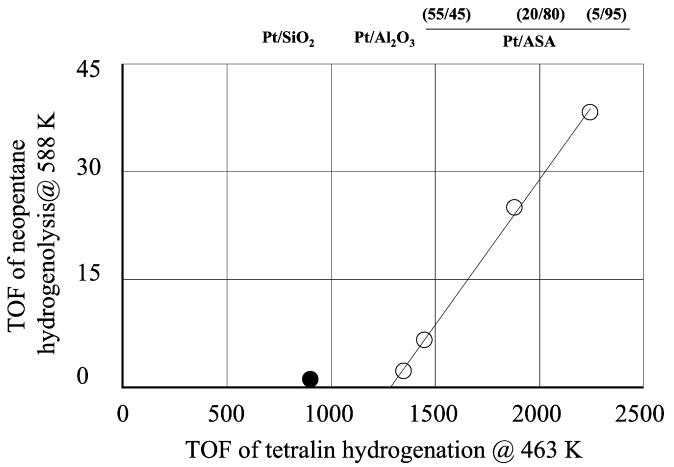

Fig. 13. Rate of the hydrogenolysis of neopentane ($T = 588$ K) vs rate of tetralin hydrogenation ($T = 463$ K) over different Pt catalysts.

reactions occurred primarily on the metal. Note that this conclusion differs from that deduced for the hydrogenation of benzene in Pt-loaded zeolite catalysts [44,45]. In this case, a significant fraction of benzene was hydrogenated at sites at the perimeter of the metal particle. At present, it is unclear to what extent the constrained local steric environment of the particles in the zeolite pores induces and creates the specific hydrogenation sites in zeolites.

The positive intercept at the x-axis indicates that more surface metal atoms are involved in hydrogenation than in hydrogenolysis, or that a second pathway exists that does not follow the hydrogenation route on the metal. In particular, the first argument points to higher ensemble size or atom specificity in hydrogenolysis reactions than in hydrogenation reactions.

3.4. Electronic state of platinum studied by XANES

The electronic properties of platinum particles on the different ASA supports were studied by X-ray absorption near edge structure (XANES). The normalized spectra in the edge region are shown in Fig. 14.

The intensity of the peak above the L_{III} edge in the XANES of the Pt/ASA catalysts varied for the different ASA carriers. This decrease in the intensity of the peak above the X-ray absorption edge clearly indicates increasing changes in the electron density of the particles with increasing electronegativity of the support. Because the particles on the ASA support are small and of similar size, as confirmed by H_2 chemisorption and from the EXAFS analysis [32], particle size differences can be excluded as the cause of the variations in the XANES findings [46]. In general, the intensity of the peak above the L_{III} edge can be related to the density of unoccupied d-states of Pt [47,48]. An interaction with an electron-withdrawing sorbate [49–51] and/or an electronegative support [52] will lead to polarization of the electrons in the metal and to a change (decrease) in the electron density in the Pt particles. For the Pt L_{III} edge, the transition from a $p_{3/2}$ ground state to partially unoccupied orbitals with $5d_{5/2}$ character in the final state is observed. In addition, the transition to final states with $5d_{3/2}$ character also are allowed at the L_{III} edge; however, these contributions can be excluded from the XANES measured at the L_{II} edge [53]. For Pt, the d-orbitals are close to the Fermi level and only partially occupied; thus, during catalytic reactions on the Pt surface, electrons from these orbitals are directly involved in the electronic interaction with the reactant molecules.

We need to mention that for all particles on the ASA support, the peak intensity above the absorption edge was smaller than the XANES of a Pt foil. This could indicate a higher overall electron density on the metal nanoclusters compared with the bulk material. Alternatively, residual hydrogen remaining on the surface after the reduction could lead to decreased intensity, but the difference spectra between the XANES of the supported particles and of the Pt foil (data not shown) confirmed the successful removal of H_2 before the experiments. In addition, Ichikuni and Iwasawa [54] found only a slight effect of hydrogen on the XANES of small platinum particles (<1.5 nm).

Thus, the changes in the intensity of the peak above the X-ray absorption edge can be attributed to variations in the electron density of the Pt particles induced from the interaction with

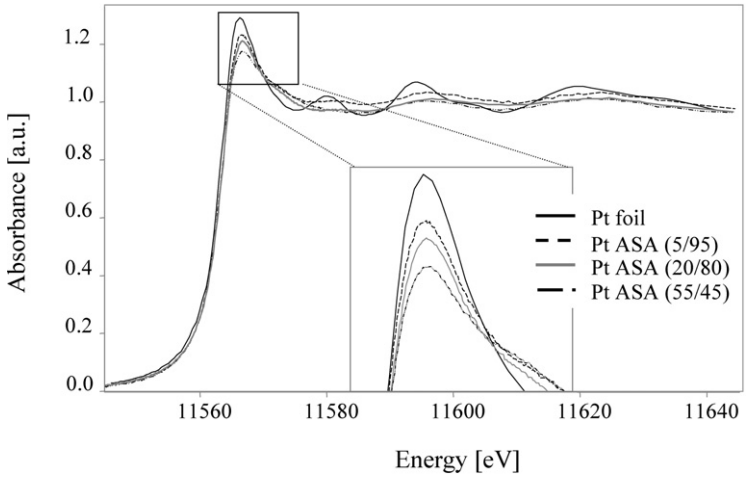

Fig. 14. Normalized XANES spectra at the L_{III} edge at 323 K in H_2.

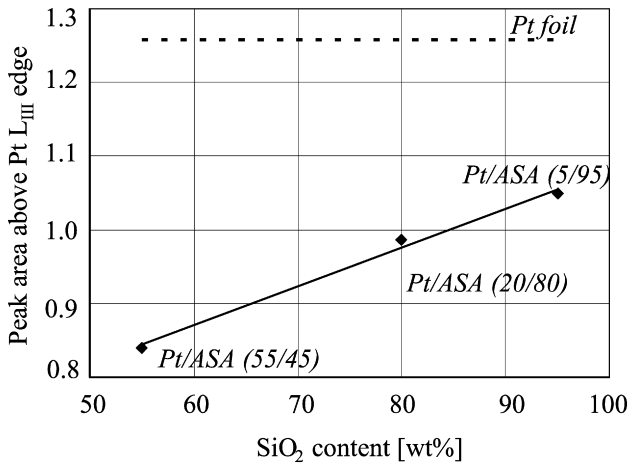

Fig. 15. Area of the peak above the Pt L_{III} edge as a function of the silica content in the support.

the acidic support. The direct proportionality between the area of the peak above the L_{III} edge and the composition of the ASA support (Fig. 15) indicates that the electron density of the Pt surface atoms decreases with increasing electronegativity of the support.

4. Conclusion

Pt supported on amorphous silica–alumina is a highly active material for hydrogenation and hydrogenolysis. The hydrogenation of tetralin and the hydrogenolysis of neopentane occur on the supported platinum particles. The reaction rates of both reactions increase with increasing intermediate electronegativity of the support as long as the support has accessible Lewis acid sites; that is, the activity increases with increasing concentration of silica in the mixed oxides. Pt supported on silica, which does not have accessible Lewis acid sites, shows the least activity for both reactions. Thus, we conclude that an efficient interaction of the support with the metal particles requires the presence of accessible Lewis acid sites. The higher the strength of these accessible Lewis acid sites, the stronger the positive effect on the metal. The higher activity is related to a lower apparent energy of activation, caused primarily by the stronger adsorption of the substrate (tetralin or neopentane) and the intermediates. This conclusion is independently supported by the preferred production of *cis*-decalin from tetralin, which is related to the strong adsorption of the intermediate.

The question arises as to why the substrate and the intermediates are more strongly bound to the metal with increasing acidity/intermediate electronegativity of the support. Both reacting molecules need the ability of the metal particle to accept electrons. This ability is strengthened with decreasing electron density on the metal particle. Thus, based on the rates, apparent energies of activation, and selectivities in the hydrogenation of tetralin, we conclude that the Pt particles show increasing electron deficiency, in parallel to the increasing acidity/intermediate electronegativity of the support.

This conclusion is strongly supported by the XANES of the ASA-supported Pt particles. With increasing acidity/intermediate electronegativity, the area of the peak above the Pt L_{III} edge increases in intensity. This increase in the area of the peak above the Pt L_{III} edge points to a higher density of the unoccupied states above the Fermi level, that is, a lower electron density in the Pt particle. Thus, overall, we conclude that the more the metal particles are depleted in electron density, the higher the acidity of the support, and that this depletion increases the strength of the adsorption of the reactants/intermediates and in turn the reaction rate of tetralin hydrogenation and neopentane hydrogenolysis.

Acknowledgments

Financial support was provided by SRTC Amsterdam. The authors thank the late Dr. W. Stork for critical discussions, Andreas Marx and Xaver Hecht for invaluable support, and HASYLAB, DESY for the beam time at the X1 experimental station.

References

[1] European Union, E.U. Directive 98/70/EC (1998).
[2] T.A. Cavanaugh, D.S. McCaffrey Jr., W.M. Gregory, Hydrocarbon Technol. Int. Summer (1994) 23.
[3] S.A. Ali, M.A.B. Siddiqui, React. Kinet. Catal. Lett. 61 (2) (1997) 363.
[4] S.L. Lee, M. De Wind, Oil Gas J. (August) (1992) 88.
[5] J.K. Minderhoud, J. Lucien, Eur. Patent 303.332 (1998).
[6] J.P. Van den Berg, J.P. Lucien, G. Germanie, G.L.B. Thielemans, Fuel Process. Technol. 35 (1993) 119.
[7] A. Stanislaus, B.H. Cooper, Catal. Rev. Sci. Eng. 36 (1) (1994) 75.
[8] B. Pawelec, R. Mariscal, R.M. Navarro, S. van Bokhorst, S. Rojas, J.L.G. Fierro, Appl. Catal. A Gen. 225 (2002) 223.
[9] R.M. Navarro, B. Pawelec, J.L.G. Fierro, P.T. Vasudevan, J.F. Cambra, B. Güemez, P.L. Arias, Fuel Process. Technol. 61 (1999) 73.
[10] H.R. Reinhoudt, R. Troost, A.D. van Langeveld, S.T. Sie, J.A.R. van Veen, J.A. Moulijn, Fuel Process. Technol. 61 (1999) 133.
[11] A. de Mallman, D. Barthomeuf, J. Chem. Phys. 87 (1990) 535.
[12] P. Chou, M.A. Vannice, J. Catal. 107 (1987) 129.
[13] S.D. Lin, M.A. Vannice, J. Catal. 143 (1993) 563.
[14] L. Le Bihan, Y. Yoshimura, Fuel 81 (2002) 491.
[15] J.L. Rousset, L. Stievano, F.J. Cadete Santos Aires, C. Geantet, A.J. Renouprez, M. Pellarin, J. Catal. 202 (2001) 163.
[16] C.C. Costa Augusto, J.L. Zotin, A. Da Costa Faro, Catal. Lett. 75 (2001) 1.
[17] Thermodynamic calculations were performed using HSC Chemistry for Windows 5.1, Outokumpu Research Oy, P.O. Box 60, FIN-28101 Pori, Finland.
[18] K. Schrage, R.L. Burwell, J. Am. Chem. Soc. 88 (1966) 4555.
[19] E.P. Martins, D.A.G. Aranda, F.L.P. Pessoa, J.L. Zotin, Braz. J. Chem. Eng. 17 (2000) 1603.
[20] A.W. Weitkamp, Adv. Catal. 18 (1968) 1.
[21] L. Fisher, V. Harlé, S. Kasztelan, Hydrotreat. Hydrocracking Oil Fractions 31 (1996) 261.
[22] A.D. Schmitz, G. Bowers, C. Song, Catal. Today 31 (1996) 45.
[23] S.M. Davis, G.A. Somorjai, in: D.A. King, D.P. Woodruff (Eds.), The Chemical Physics of Solid Surfaces and Heterogeneous Catalysts, vol. 4, Elsevier, Amsterdam, 1982, p. 271.
[24] J.R. Anderson, N.R. Avery, J. Catal. 16 (1967) 315.
[25] D.C. Koningsberger, M.K. Oudenhuijzen, J. de Graaf, J.A. van Bokhoven, D.E. Ramaker, J. Catal. 216 (2003) 178.
[26] H. Yoshitake, Y. Iwasawa, J. Phys. Chem. 95 (1991) 7368.
[27] H. Yoshitake, Y. Iwasawa, J. Catal. 131 (1991) 276.
[28] H. Yoshitake, Y. Iwasawa, J. Phys. Chem. 96 (1992) 1329.
[29] D.R. Short, A.N. Mansour, J.W. Cook Jr., D.E. Sayers, J.R. Katzer, J. Catal. 82 (1983) 299.

[30] C. Woltz, A. Jentys, J.A. Lercher, J. Catal. 237 (2006) 337.
[31] K.V. Klementiev, VIPER for Windows, freeware: http://www.desy.de/~klmn/viper.html.
[32] M.F. Williams, B. Fonfé, C. Sievers, A. Abraham, J.A. van Bokhoven, A. Jentys, J.A.R. van Veen, J.A. Lercher, Hydrogenation of tetralin on silica–alumina-supported Pt catalysts, I: Physicochemical characterization of the catalytic materials, J. Catal. 251 (2007) 485.
[33] R.T. Sanderson, Polar Covalence, Academic Press, 1983.
[34] S.D. Lin, C. Song, Catal. Today 31 (1996) 93.
[35] X.D. Zhan, J.A. Guin, Energy Fuels 8 (1994) 1384.
[36] A. Stanislaus, B.H. Cooper, Catal. Rev. Sci. Eng. 36 (1994) 75.
[37] M. Koussathana, D. Vamvouka, H. Economon, X. Verykios, Appl. Catal. 77 (1991) 283.
[38] G.C. Bond, M.A. Keane, H. Kral, J.A. Lercher, Catal. Rev. Sci. Eng. 42 (2000) 323.
[39] W. Patterson, J.J. Rooney, J. Catal. 146 (1994) 310.
[40] G.C. Bond, A.D. Hooper, J.C. Slaa, A.O. Taylor, J. Catal. 163 (1996) 319.
[41] K.E. Foger, J.R. Anderson, J. Catal. 54 (1978) 318.
[42] S.T. Homeyer, Z. Karpinski, W.M.H. Sachtler, J. Catal. 123 (1990) 60.
[43] A.K. Galwey, Thermochim. Acta 294 (1997) 205.
[44] L. Simon, J.G. van Ommen, A. Jentys, J.A. Lercher, J. Catal. 201 (2001) 60.
[45] L. Simon, J.G. van Ommen, A. Jentys, J.A. Lercher, J. Catal. 203 (2001) 434.
[46] D. Bazin, J.J. Rehr, J. Phys. Chem. B 107 (2003) 12398.
[47] A.N. Mansour, J.W. Cook, D.E. Sayers, J. Phys. Chem. 88 (1984) 2330.
[48] A.L. Ankudinov, J.J. Rehr, J. Chem. Phys. 116 (2001) 1911.
[49] M.G. Samant, M. Boudart, J. Phys. Chem. 95 (1991) 4070.
[50] T. Kubota, K. Asakura, Y. Iwasawa, Catal. Lett. 46 (1997) 141.
[51] A. Jentys, L. Simon, J.A. Lercher, J. Phys. Chem. B 104 (2000) 9411.
[52] J.T. Miller, B.L. Mojet, D.E. Ramaker, D.C. Koningsberger, Catal. Today 62 (2000) 101.
[53] D. E Ramaker, B.L. Mojet, M.T.G. Oostenbrink, J.T. Miller, D.C. Koningsberger, Phys. Chem. Chem. Phys. 1 (1999) 2293.
[54] N. Ichikuni, Y. Iwasawa, Catal. Lett. 20 (1993) 87.